RAPID COMMUNICATIONS

PHYSICAL REVIEW A VOLUME 45, NUMBER 2 15 JANUARY 1992

Microscopic-growth morphologies in binary systems

Rong-Fu Xiao, J. Iwan D. Alexander, and Franz Rosenberger
Center for Microgravity and Materials Research, University of Alabama in Huntsville, Huntsville, Alabama 35899
(Received 7 October 1991)

Microscopic solidification morphologies of binary systems are simulated with a Monte Carlo model that accounts for bulk diffusion, attachment and detachment kinetics, and surface diffusion. Through variation of interaction energies and undercooling, a broad range of microstructures is obtained, including eutectic systems and layered and ionic compounds.

PACS number(s): 61.50.Cj, 05.50.+q, 81.30.Fb, 68.45.Ax

We introduce a powerful Monte Carlo (MC) model to simulate the growth morphologies and microstructures of binary crystals. Explicit consideration is given to mutual interactions between like and unlike particles at the solid-liquid interface. Previous treatments of the morphologies of binary systems have either been macroscopic continuum theories, which deal with dilute binary alloys [1] or binary eutectics [2], or microscopic theories [3–7]. Apart from the work of Karma [8], microscopic theories have involved statistical models that ignore bulk diffusive transport. Although restricted to systems with two nonfaceting pure phases, Karma's work represents a significant step toward understanding steady and unsteady growth morphologies in eutectic systems.

Our MC model deals with an isothermal two-component system that is contained in a rectangular region with a square grid. Initially, most of the region is occupied by a liquid that consists of particles A and B (with concentrations given by the mole fractions X_A and $X_B=1-X_A$), which occupy each grid point according to a preset concentration ratio. Diffusion in the liquid is modeled by random walks on the grid [9]. Periodic boundary conditions are used on the grid sidewalls. The system temperature T is less than the equilibrium melting temperature T_e, i.e., the liquid is undercooled by $\Delta T=T_e-T$. In order to "seed" solidification, the grid initially has two base lines that are considered as solid, and that are fully but randomly occupied by either A or B particles according to the bulk liquid's X_A. Depending on the simulation conditions (see below), solidification may lead to a solid solution or two solid phases. Lattice mismatches between adjacent solid phases are proscribed. Although we invoked the solid-on-solid assumption [10] in the solidification process, it is not required by our formulation.

In state s_1, the system contains N particles of which N_s are solid and N_l liquid. After a time step Δt, the system changes to state s_2, in which M particles in the liquid phase have become solid. The master equation for this transition is

$$\frac{dP(s_2,t)}{dt}=\sum_{s_1}[k(s_1,s_2)P(s_1,t)-k(s_2,s_1)P(s_2,t)]\,, \tag{1}$$

where $k(s_1,s_2)$ and $k(s_2,s_1)$ are the transition probabilities for $s_1\rightarrow s_2$ and $s_2\rightarrow s_1$, respectively. The individual state probability is

$$P(s_j,t)=\Omega_{s_j}\exp\left[-\beta\left[H\{s_j\}-\sum_i^N\mu_{s_j}^i\right]\right],\quad j=1,2\,, \tag{2}$$

where $H\{s_j\}$ and $\mu_{s_j}^i$ are the Hamiltonian and site-dependent chemical potential for state s_j, respectively, and $\beta=1/kT$, where k is Boltzmann's constant, and the Ω_{s_j} are the product of individual vibration factors Ω_i. For detailed balance, $dP/dt=0$ and the overall attachment probability is

$$P^+=\frac{k(s_1,s_2)}{k(s_1,s_2)+k(s_2,s_1)}=\frac{\chi}{1+\chi}\,, \tag{3}$$

with

$$\chi=\frac{P(s_2)}{P(s_1)}=\prod_{i=1}^{M}\chi_i=\prod_{i=1}^{M}\Omega_i\exp[-\beta(\Delta E_i-\Delta\mu_i)]\,, \tag{4}$$

where ΔE_i and $\Delta\mu_i$ are the change of internal energy and chemical potential, respectively, for the transition. $\Delta\mu_j$ can be calculated from the undercooling ΔT and the interfacial concentration difference ΔX_i^L between the melt X_i^L and equilibrium concentration X_e [11]:

$$\Delta\mu_i=\Delta\mu_i^T+\Delta\mu_i^X=\frac{L_p}{T_e}\Delta T+\frac{kT_e}{X_e}\Delta X_i^L\,, \tag{5}$$

where L_p is the latent heat of solution (with p designating the specific solid phase).

The individual attachment probability for particle i is

$$P_i^+=\frac{\chi_i}{1+\chi_i}=\frac{\exp\{-\beta[(\Delta E_{i0}-\Delta E_i)-\Delta\mu_i]\}}{1+\exp\{-\beta[(\Delta E_{i0}-\Delta E_i)-\Delta\mu_i]\}}\,, \tag{6}$$

where the transition energy change $\Delta E_{i\omega}$ ($\omega=A$ or B) is (for solid-solid particle interactions only)

$$\Delta E_{i\omega}=\phi_{\omega\omega 1}(n_{\omega\omega 1}+\epsilon_{\omega\omega 2}n_{\omega\omega 2}+\epsilon_{\omega\bar{\omega}1}n_{\omega\bar{\omega}1}+\epsilon_{\omega\bar{\omega}2}n_{\omega\bar{\omega}2})\,, \tag{7}$$

with $\phi_{\omega\omega 1}\equiv\phi_{\omega\omega}$ denoting the pair (nearest-neighbor) interaction energy which is assumed $\sim 1/r^m$ such that, through appropriate choice of the exponent m, various types of interaction can be approximated. The $n_{\omega\omega 1}$, $n_{\omega\omega 2}$, $n_{\omega\bar{\omega}1}$, and $n_{\omega\bar{\omega}2}$ represent the number of first, second, "like," and "unlike" nearest neighbors, respectively. The ϵ terms denote the normalized bond strengths

$$\epsilon_{\omega\omega 2}=\phi_{\omega\omega 2}/\phi_{\omega\omega 1},\quad \epsilon_{\omega\bar{\omega}1}=\phi_{\omega\bar{\omega}1}/\phi_{\omega\omega 1},\quad \epsilon_{\omega\bar{\omega}2}=\phi_{\omega\bar{\omega}2}/\phi_{\omega\omega 1}\,.$$

Thus the energy change associated with the attachment of a particle i to a kink site on the solid surface is

$$\Delta E_{i0}=\phi_{\omega\omega 1}[n_{10}\xi_1+n_{20}\xi_2\epsilon_{\omega\omega 2}+n_{10}(1-\xi_1)\epsilon_{\omega\bar{\omega}1} +n_{20}(1-\xi_2)\epsilon_{\omega\bar{\omega}2}], \quad (8)$$

where n_{10} and n_{20} are the number of occupied nearest and second-nearest neighbors for a kink site, $\xi_1=n_{\omega\omega 1}/(n_{\omega\omega 1}+n_{\omega\bar{\omega}1})$, and $\xi_2=n_{\omega\omega 2}/(n_{\omega\omega 2}+n_{\omega\bar{\omega}2})$.

The probability P_i^d for selecting a specific interfacial solid particle to detach from the surface can be calculated from E_i, the energy configuration [9] of site i, as

$$P_i^d=\frac{\exp(-\beta E_i)}{\sum_i \exp(-\beta E_i)}, \quad (9)$$

and thus a particle with fewer solid neighbors will have a larger detachment probability.

For surface diffusion, we assume [9] that the diffusion rate depends on the occupation condition of both the site i that particle occupies and the potential jump site j:

$$K_{ij}=\nu_s \exp(-\Delta E_{ij}\beta), \quad (10)$$

where ν_s is the surface vibration factor and ΔE_{ij} is the activation energy. Note that, although there is no dimensional limitation in our MC formulations, in this paper we only consider a two-dimensional simulation.

The simulation begins by calculating the overall attachment probability P^+. A random number R is generated. If $R<P^+$, an attachment is considered. A "liquid particle" (either A or B, depending on the mole fraction X_i) is selected at the interface. Then the probability $P_{i\omega}^+$ [Eq. (6)] is calculated to decide whether attachment occurs. If the particle attaches, the local configuration is changed and the overall P^+ is recalculated. If the liquid particle does not attach, it will diffuse away by either surface or bulk diffusion (i.e., random walk), until it reaches the top of the region, whereupon its motion is no longer recorded [12], or reaches an interfacial site. If $R>P^+$, a detachment is considered. A "solid particle" is chosen on the interface and its detachment probability calculated according to Eq. (9). If detachment occurs, diffusion ensues, just as for particles that failed to attach. Throughout the simulation, a registration scheme is used to calculate the concentration distribution in the liquid [9]. The local mole fraction X_A is updated frequently to ensure the correct selection of the liquid particle during the simulation. Furthermore, the interfacial X_A data are used for the calculation of the concentration term in Eq. (5). The above process is repeated until the solid has reached a preset size.

The following preliminary results involve systems with $X_e=0.5$, equal interaction between like particles (i.e., $\phi_{AA}=\phi_{BB}$), and various A-B interactions, including model ionic interactions and different values of the interaction exponent m. Figure 1 shows results obtained at a fixed undercooling $\Delta\mu^T/kT=0.5$. The solid and open boxes (for Figs. 1 and 2 only) represent component A and B in the solid phases, respectively. Figure 1(a) presents a case with equal interaction between unlike and like particles, $\phi_{\omega\omega 1}/kT=2.3$, and where the strength of second-neighbor

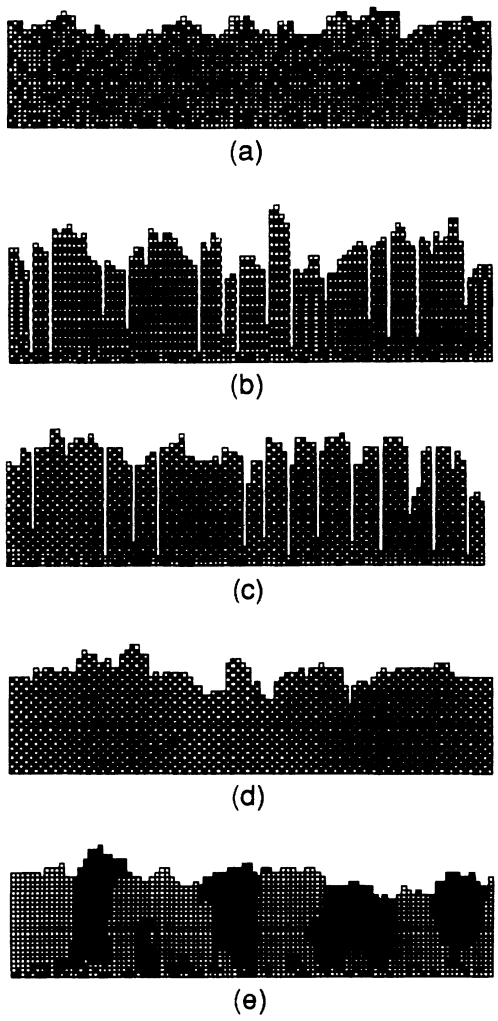

FIG. 1. Microscopic growth morphologies of binary crystals at fixed undercooling $\Delta\mu^T/kT=0.5$ and various interaction conditions: (a) $\phi_{\omega\omega 1}/kT=2.3$, $\epsilon_{\omega\bar{\omega}1}=1.0$, $\epsilon_{\omega\omega 2}=\epsilon_{\omega\bar{\omega}2}=0.1$; (b) $\phi_{\omega\omega 1}/kT=-2.3$, $m=1$; (c) $\phi_{\omega\omega 1}/kT=-2.3$, $m=3$; (d) $\phi_{\omega\omega 1}/kT=-2.3$, $m=6$; (e) $\phi_{\omega\omega 1}/kT=2.3$, $\epsilon_{\omega\bar{\omega}1}=\epsilon_{\omega\omega 2}=0.1$, $\epsilon_{\omega\bar{\omega}2}=0.05$.

interaction is 10% of the first-nearest-neighbor interaction (equivalent to $m\approx 6$). One sees that no component segregation results and the particle distribution in the solid phase is random. For Figs. 1(b)–1(d), the interaction energies between neighboring particles are all of ionic type, with $\phi_{\omega\omega 1}/kT=-2.3$, $\epsilon_{\omega\omega 1}=-\epsilon_{\omega\bar{\omega}1}=1.0$. The interaction exponent was varied from $m=1$ [Fig. 1(b)] to $m=3$ [Fig. 1(c)] and $m=6$ [Fig. 1(d)]. As can be seen from Fig. 1(b), the particles with Coulomb potential ($\sim 1/r$) prefer to pack in layers and columns of like charge. With increasing m, the crystal structure changes from layers to two-dimensional NaCl-like patterns [Fig. 1(c) and 1(d)], with a critical value of $m=2$ for the turnover. We found that for $m=1$, a crystal can have NaCl-like characteristics only when more distant-neighbor interactions are included, which is consistent with the long-range interactions in ionic crystals. This result is of in-

terest, since it contrasts with those of earlier simulations [7] of ionic crystal growth that considered only first-nearest neighbors and neglected bulk diffusion. In Fig. 1(e) the interaction energies between neighboring particles are $\phi_{\omega\omega 1}/kT=2.3$, $\epsilon_{\omega\bar{\omega}1}=\epsilon_{\omega\omega 2}=0.1$, and $\epsilon_{\omega\bar{\omega}2}=0.05$. This reduction of the nearest-neighbor interaction between unlike particles to 10% of that between like particles results in a lamellar structure of two solid phases that are pure A and B, respectively. If a particle A, by chance, lands at a surface site with mostly solid B neighbors, the weaker attraction between unlike particles will result in a low attachment probability and a large detachment probability. The A particle will probably leave that site and randomly walk in the liquid until it finds a more favorable surface site with more particles of the same type.

In addition to the interaction energy, the undercooling can also greatly influence the crystal-growth morphology. This is illustrated in Fig. 2. Here the interaction energies are all fixed ($\phi_{\omega\omega 1}/kT=3.9$, $\epsilon_{\omega\bar{\omega}1}=\epsilon_{\omega\omega 2}=0.1$, and $\epsilon_{\omega\bar{\omega}2}=0.05$). At low undercooling, $\Delta\mu^T/kT=0.1$, a lamellar microstructure forms [Fig. 2(a)], which exhibits a wide spacing (≈ 120 lattice constants) with local "facets," i.e., regions of low surface roughness. In addition, deep grooves are formed near the three-phase junction, where solid A, solid B, and the liquid meet. At $\Delta\mu^T/kT=0.5$ [Fig. 2(b)], the lamellar spacing decreases. At $\Delta\mu^T/kT=5.0$ [Fig. 2(c)], not only does the spacing decrease, but the interfaces also roughen. In addition, the grooves at the junctions grow out and eventually disappear. This is fundamentally different from growth behavior observed by Karma [8], which is subject to the constraint of triple-point equilibrium. Finally, at infinite undercooling [Fig. 2(d), $\Delta\mu^T/kT=\infty$] there is no phase ordering. This is because the attachment probability is too high to allow particles to redistribute. Under these circumstances, the solid-liquid interface becomes rough, and significantly increases in width.

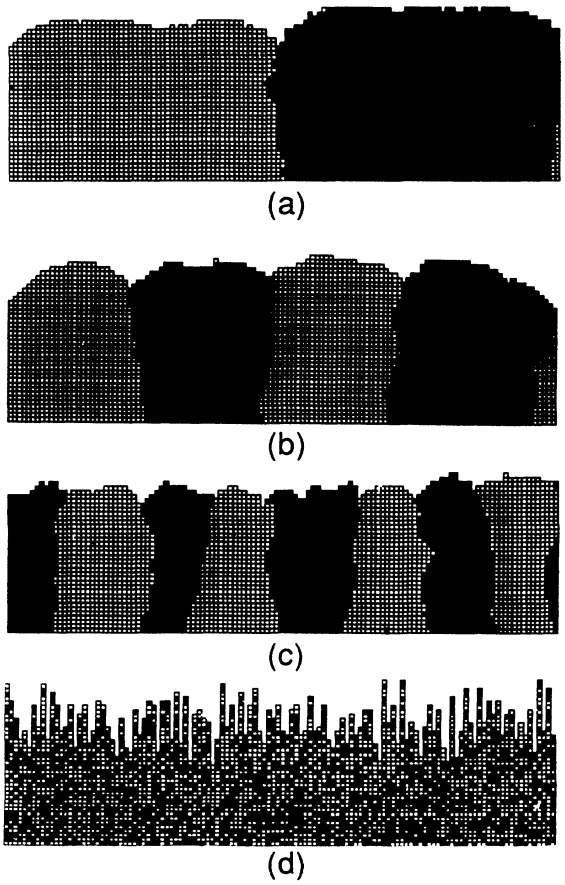

FIG. 2. Microscopic growth morphologies of binary crystals at fixed interaction energies $\phi_{\omega\omega 1}/kT=3.9$, $\epsilon_{\omega\bar{\omega}1}=\epsilon_{\omega\omega 2}=0.1$, $\epsilon_{\omega\bar{\omega}2}=0.05$, and increasing undercooling: (a) $\Delta\mu^T/kT=0.1$; (b) $\Delta\mu^T/kT=0.5$; (c) $\Delta\mu^T/kT=5.0$; (d) $\Delta\mu^T/kT=\infty$.

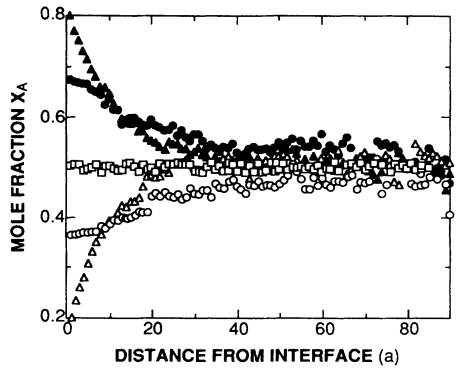

FIG. 3. Mole fraction X_A along the growth direction at the center of lamella A (lower half) and B (upper half). ●,○ correspond to Fig. 2(a); ▲,△ to Fig. 2(b); and □ to Fig. 2(d). Distance in units of lattice constant a.

The coupling between local composition and solid morphology is illustrated in Fig. 3, which shows profiles of X_A, the mole fraction, along the growth direction for conditions corresponding to Figs. 2(a), 2(b), and 2(d). Two profiles are plotted for each situation: one lies along the center of the solid phase A, the other lies along the center of phase B. One sees that X_A has a minimum ahead of the A-rich phase and a maximum in front of the B-rich phase, reflecting, respectively, the depletion and rejection of A at these phases. This nonuniformity in concentration dimin-

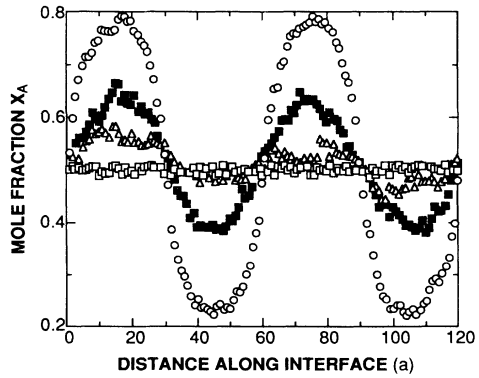

FIG. 4. Mole fraction X_A parallel to the solid-liquid interface of Fig. 2(b) at $2a$ (○), $10a$ (■), $20a$ (△), and $50a$ (□) into the liquid. Distance in units of lattice constant a.

ishes with distance from the solid-liquid interface. Figure 3 also shows that the segregation is highly dependent on the growth conditions. With increasing undercooling, there will be less of a chance for liquid particles to relax. This kinetic effect not only results in a narrower lamellar spacing (Fig. 2), but also narrower and steeper concentration boundary layers. The local character of segregation is further illustrated in Fig. 4 for the case of Fig. 2(b) by composition profiles parallel to the interface at distances of 2, 10, 20, and 50 lattice constants into the melt. As can be seen in this figure, the melt concentration periodically changes with the lamellar solid phases. With increasing distance into the melt, the concentration distribution gradually becomes uniform.

In conclusion, we have shown via a MC simulation, the importance of interfacial mass segregation and melt diffusion in the ordering of binary systems during solidification. Depending on the interaction energies between particles, the microscopic growth structures range from complete mixing to complete segregation. For the same interaction energy, the growth morphologies can also be greatly affected by undercooling. As undercooling increases, the interphase spacing of lamellar eutectics decreases. Since we have chosen to describe the growth of two-component systems using a combination of random walk to model bulk diffusion, and calculated transition probabilities to model microscopic surface kinetics, our results are limited to length scales characterized by these processes. At this stage, our results can be used only to qualitatively predict morphological and microstructural textures (for example, the relationship between velocity and lamellar eutectic spacing); direct predictions of morphologies in macroscopic systems cannot be made without either increasing the size of the systems we simulate (which would be computationally inefficient) or coarse graining in such a way as to retain those aspects of microscopic kinetics that are manifested in macroscopic morphologies [13].

[1] S. R. Coriell, G. B. McFadden, and R. F. Sekerka, Annu. Rev. Mater. Sci. **15**, 119 (1985).

[2] K. A. Jackson and J. D. Hunt, Metall. Trans. **236**, 1129 (1966); R. Trivedi, P. Magnin, and W. Kurz, Acta Metall. **35**, 971 (1987).

[3] H. Pfeiffer, T. Klupsch, and W. Haubenreisser, *Microscopic Theory of Crystal Growth* (Akademie, Berlin, 1989), p. 128.

[4] H. Müller-Krumbhaar, in *Monte Carlo Methods in Statistical Physics,* edited by K. Binder (Springer, Berlin, 1979), p. 295, and references therein.

[5] A. A. Chernov and J. Lewis, J. Phys. Chem. Solids **24**, 2185 (1967).

[6] T. A. Cherepanova, A. V. Shirin, and V. T. Borisov, in *Industrial Crystallization,* edited by J. W. Mullin (Plenum, New York, 1976), p. 113; Kristallografiya **22**, 260 (1977) [Sov. Phys. Crystallogr. **22**, 147 (1977)]; T. A. Cherepanova, Phys. Status Solidi **58**, 469 (1980); **59**, 371 (1980); T. A. Cherepanova and J. B. Dzelme, Cryst. Res. Technol. **16**, 399 (1981); T. A. Cherepanova and A. S. Koziejowska, Phys. Status Solidi (a) **77**, 35 (1983).

[7] T. A. Cherepanova, J. P. Van der Eerden, and P. Bennema, J. Cryst. Growth **44**, 537 (1978).

[8] A. Karma, Phys. Rev. Lett. **59**, 71 (1987); in *Solidification Processing of Eutectic Alloys,* edited by D. M. Stefanescu, G. J. Abbaschian, and R. J. Bayuzick (Metallurgical Society, Warrendale, PA, 1988), p. 35.

[9] R.-F. Xiao, J. Iwan D. Alexander, and F. Rosenberger, Phys. Rev. A **38**, 2447 (1988); J. Cryst. Growth **100**, 313 (1990); Phys. Rev. A **43**, 2977 (1991).

[10] D. E. Temkin, in *Crystallization Processes,* edited by N. N. Sirota, F. K. Gorskii, and V. M. Varikash (Consultant Bureau, New York, 1966), p. 15.

[11] R.-F. Xiao, J. I. D. Alexander, N.-B. Ming, and F. Rosenberger (unpublished).

[12] To set the distance between the interface and the top of the region we increased the separation until we reached a point at which further increases in separation no longer affected the growth morphology [9]. Near the top of the region the melt concentration is uniform (see Figs. 3 and 4). Here the motion of walkers is no longer affected by the presence of the interface. Hence, to save CPU time, we ignore the walker after it has reached this point even though it will eventually return to the interface. This boundary condition is analogous to the so-called quasi-steady assumption [P. M. Adornato and R. A. Brown, J. Cryst. Growth **80**, 155 (1987)] used in continuum models of directional solidification.

[13] D. E. Temkin, J. Cryst. Growth **52**, 299 (1981), discusses the relationship between microscopic growth and the continuum description of two-component growth; shows that the transition probabilities can be used to develop expressions for fluxes, which in the limit satisfy the continuum boundary conditions for two-component growth; and gives some approximate equations which demonstrate the continuum limit for atomically rough interfaces.

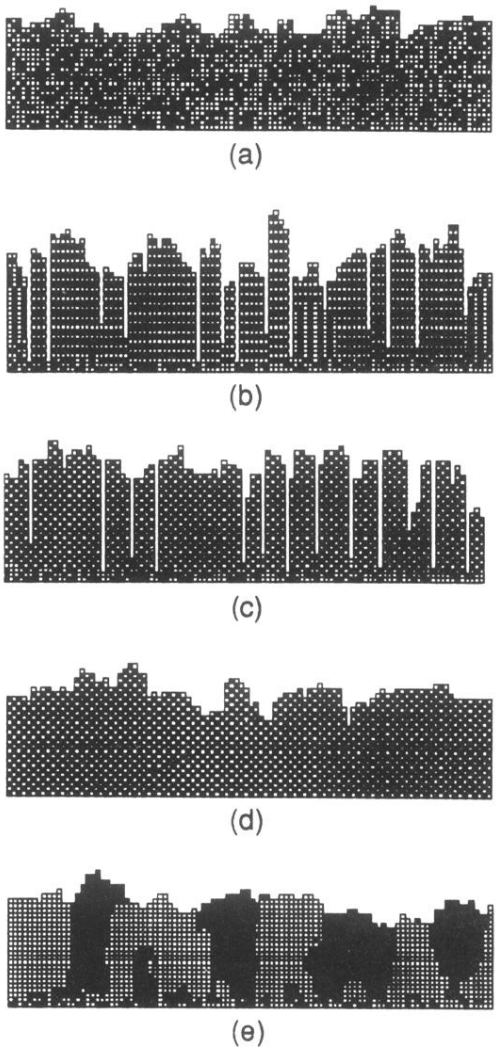

FIG. 1. Microscopic growth morphologies of binary crystals at fixed undercooling $\Delta\mu^T/kT=0.5$ and various interaction conditions: (a) $\phi_{\omega\omega 1}/kT=2.3$, $\epsilon_{\omega\bar{\omega}1}=1.0$, $\epsilon_{\omega\omega 2}=\epsilon_{\omega\bar{\omega}2}=0.1$; (b) $\phi_{\omega\omega 1}/kT=-2.3$, $m=1$; (c) $\phi_{\omega\omega 1}/kT=-2.3$, $m=3$; (d) $\phi_{\omega\omega 1}/kT=-2.3$, $m=6$; (e) $\phi_{\omega\omega 1}/kT=2.3$, $\epsilon_{\omega\bar{\omega}1}=\epsilon_{\omega\omega 2}=0.1$, $\epsilon_{\omega\bar{\omega}2}=0.05$.

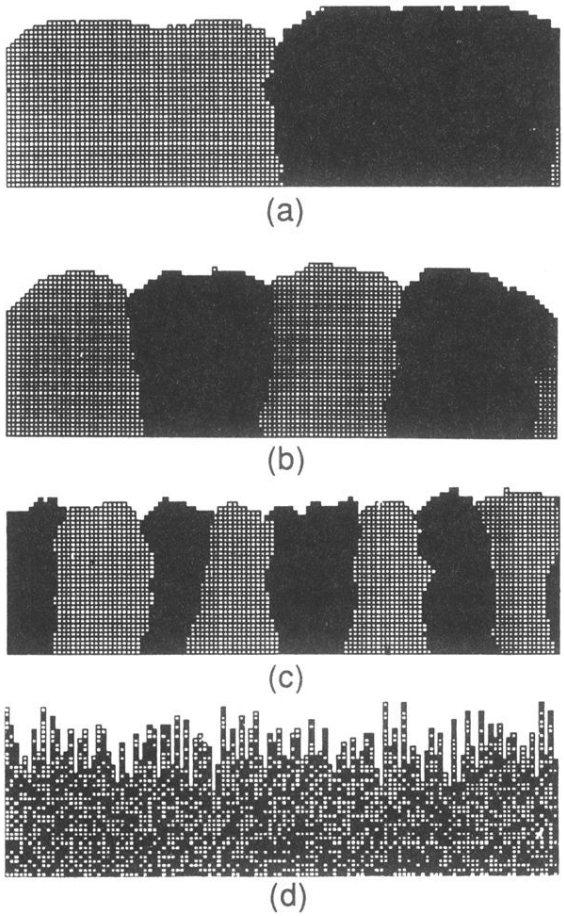

FIG. 2. Microscopic growth morphologies of binary crystals at fixed interaction energies $\phi_{\omega\omega 1}/kT=3.9$, $\epsilon_{\omega\bar{\omega}1}=\epsilon_{\omega\omega 2}=0.1$, $\epsilon_{\omega\bar{\omega}2}=0.05$, and increasing undercooling: (a) $\Delta\mu^T/kT=0.1$; (b) $\Delta\mu^T/kT=0.5$; (c) $\Delta\mu^T/kT=5.0$; (d) $\Delta\mu^T/kT=\infty$.